Modeling and Control Design of a Current-Mode Controlled Flyback Converter with Optocoupler Feedback

W. Kleebchampee and C. Bunlaksananusorn
Faculty of Engineering,
King Mongkut's Institute of Technology Ladkrabang,
Bangkok, Thailand
e-mail: kbchanin@kmitl.ac.th

Abstract— **In this paper, modeling and control design of a current-mode controlled flyback converter with optocoupler feedback is presented. Small-signal models of the converter operating in Continuous Conduction Mode (CCM) and Discontinuous Conduction Mode (DCM) are derived and used in control design of the prototype converters, with the results confirmed by experiment.**

Keywords-flyback converter; current-mode control; modeling; control design

I. INTRODUCTION

A flyback converter is used extensively in "off-the-line" power supplies for modern office equipment, e.g. computer monitors, notebooks, printers, etc., due to its compactness and cost effectiveness. In these applications, a peak current-mode control is usually used to regulate an output voltage as shown in Fig. 1. The output voltage feedback is implemented by the TL431 error amplifier, which is a low-cost three-terminal device with a reference voltage included inside the package, configured to work with an optocoupler, which provides an isolated control signal to a current-mode control stage. For the flyback converter in Fig. 1 to be stable and have satisfactory steady state and dynamic performances throughout its operating range, the feedback controller, which in this case comprises of Z_1, Z_2, R_{C3}, and C_{C3}, must be carefully designed. To facilitate the controller design, the converter's small-signal model is needed. Modeling and controller design of a flyback converter is proposed in [1], in which the authors derive the converter's reduced model and use it in the controller design through the closed-form formulas that relate the output specifications to the controller parameters. This quantitative approach is, however, only applicable to a PI controller, which has limited practical usage due to its inability in suppressing high frequency noises. Moreover, accuracy of these closed-form equations is somewhat questionable because they are derived from the simplified converter model. Recently, accurate modeling methods for the PWM converters [2], current-mode control [3,4], and optocoupler feedback controller [5] have been developed. By applying these modeling techniques to the respective stages of the converter in Fig. 1, the overall system can be modeled and the transfer function suitable for the controller design derived. The controller design can then be proceeded using conventional Bode plots, which is applicable to a wide range of controllers, not restricted to just the PI one. Based on the described concept, this paper presents modeling and control design of a current-mode controlled flyback converter with optocoupler feedback, where both cases of Continuous Conduction Mode (CCM) and Discontinuous Conduction Mode (DCM) are considered.

II. CIRCUIT OPERATION

The operation of the flyback converter in Fig. 1 can be described as follows. In each switching period, the constant-frequency clock signal sets the RS flip flop, turning on the power MOSFET, M_1, and enabling energy storage in the flyback transformer. As soon as the sensed switch current, v_s, reaches the control signal, v_c, the RS flip flop is reset, M_1 is turned off, and the stored energy is released to the load. The output voltage, v_o, is fed back to the TL431 error amplifier, through the resistive divider comprising of R_{D1} and R_{D2}. When the sensed output voltage, v_{KD}, is greater than the internal reference voltage of the TL431, the output voltage of the error

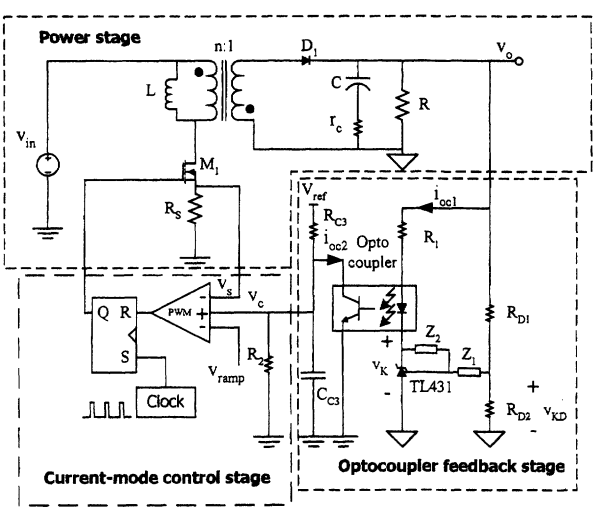

Figure 1. Current-mode controlled flyback converter with optocoupler feedback.

0-7803-9296-5/05/$20.00 © 2005 IEEE

amplifier, v_K, is decreased, hence increasing the optocoupler's diode current, i_{oc1}, as well as the optocoupler's transistor current, i_{oc2}. The increase in i_{oc2} causes the control signal, v_c, to decrease and thus v_s reaches v_c sooner, thereby decreasing the duty cycle of the power MOSFET, d. On the contrary, when v_{KD} is smaller than the internal reference voltage of the TL431, d will be increased. Through the aforementioned regulation mechanism, v_o can be maintained at the desired level against changes in the input voltage and/or load current. It should be noted that the compensation ramp, V_{ramp}, is used when the converter operates with $d > 0.5$ to prevent instability.

III. Small Signal Modeling

The flyback converter in Fig. 1 is composed of three stages. The small-signal model of each stage is described below.

A. *Flyback Power Circuit*

Referring the power circuit to the secondary, the equivalent buck-boost converter, with the input voltage of V_{in}/n and inductance of L/n^2, is obtained. Replacing the power MOSFET and diode in the equivalent buck-boost circuit by the small-signal PWM switch models in CCM and DCM [2], the small-signal equivalent circuits are obtained as shown in Figs. 2a and 2b respectively. In the figures, the capital letters denote DC values and the caret the small-signal variations. In the CCM circuit, $V_{ap} = (V_{in}/n) + V_o$ and $I_c = I_L$. In the DCM circuit, $g_i = M^2/R$, $k_i = 2MV_o/DR$, $g_f = 2M/R$, $k_o = 2V_o/DR$ and $g_o = 1/R$, where $M = V_o/V_{in} = nD\sqrt{R/2Lf_s}$. D and f_s are the duty cycle and switching frequency respectively. The small-signal equivalent circuits have two input variables, $\hat{v}_{in}(s)$ and $\hat{d}(s)$, and two output variables, $\hat{i}_L(s)$ and $\hat{v}_o(s)$. Hence, the following four transfer functions can be derived from the equivalent circuits:

- The line-to-output transfer function,

$$G_{vv}(s) = \left.\frac{\hat{v}_o(s)}{\hat{v}_{in}(s)}\right|_{\hat{d}(s)=0}$$

- The line-to-inductor current transfer function,

$$G_{iv}(s) = \left.\frac{\hat{i}_L(s)}{\hat{v}_{in}(s)}\right|_{\hat{d}(s)=0}$$

- The duty cycle-to-output transfer function,

$$G_{vd} = \left.\frac{\hat{v}_o(s)}{\hat{d}(s)}\right|_{\hat{v}_{in}(s)=0}$$

- The duty cycle-to-inductor current transfer function,

$$G_{id}(s) = \left.\frac{\hat{i}_L(s)}{\hat{d}(s)}\right|_{\hat{v}_{in}(s)=0}$$

As shown later in Section IV, only $G_{vd}(s)$ and $G_{id}(s)$ are required in derivation of a control-to-output transfer function used for control design.

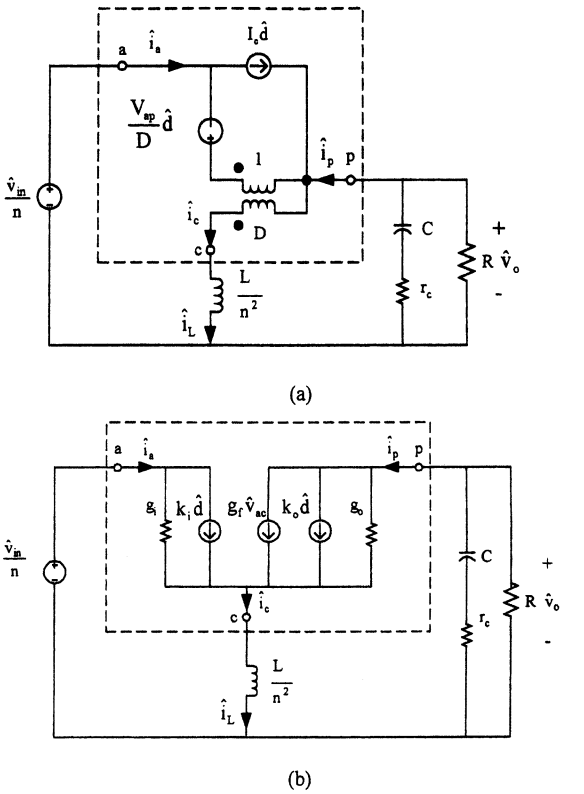

Figure 2. Small-signal models of a flyback power circuit (a) CCM (b) DCM.

B. *Current-Mode Control*

A current-mode control circuit and its associated waveform in CCM are shown in Fig. 3(a) and 3(b) respectively. The constant-frequency clock signal sets an RS flip-flop, which turns on the power MOSFET causing i_L to ramp up. When the sensed inductor current, $v_s = R_s i_L$, is equal to v_c, the power MOSFET is turned off and i_L starts to ramp down. If the converter is to operate with $d > 0.5$, V_{ramp} will be needed to prevent potential instability. In the figure, S_e, S_n, and S_f are slope of v_{ramp}, slope of i_L during the power MOSFET's turn-on and slope of i_L during the power MOSFET's turn-off respectively. It can be seen from the waveform in Fig. 3(b) that d is governed by v_c, i_L, and slopes of i_L and v_{ramp}. Hence, a small-signal model of current mode control must implicitly or explicitly relates changes in d in terms of changes in these governing variables. In recent years, many CCM current-control models have been proposed [6]. The model by Ridley [2] however seems to be most widely accepted due to its good accuracy, and is given by

$$\hat{d} = F_m\left(\hat{v}_c - R_s H_e(s)\hat{i}_L + k'_f\,\hat{v}_{on} + k'_r\,\hat{v}_{off}\right) \qquad (1)$$

where F_m is a gain of the current-mode control modulator, K'_r and K'_f are a gain that represents respectively the effect of the inductor voltage during the power MOSFET's turn on ($\hat{v}_{on}$) and turn-off ($\hat{v}_{off}$) on the slope of i_L, and $H_e(s)$ is a second-order continuous-time function that models the sampling

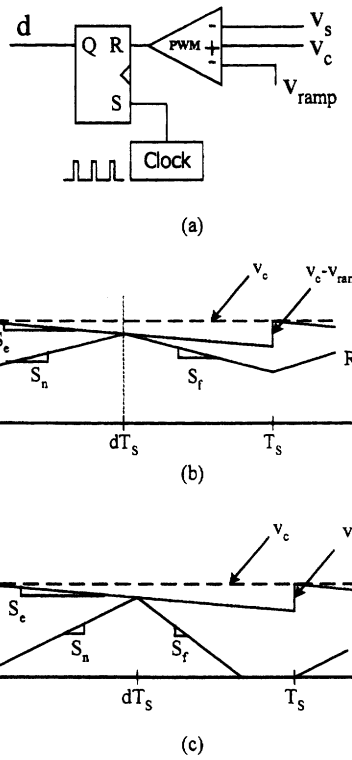

Figure 3. (a) Current-mode control circuit (b) Waveforms in CCM (c) Waveforms in DCM.

action of the current loop. $H_e(s)$, in effect, causes a second-order gain peaking at half the switching frequency $f_s/2$. Hence, the controller selected for output voltage regulation must be able to provide adequate gain attenuation at this frequency or else instability may occur. The values of F_m, K'_r, K'_f and $H_e(s)$ for a CCM flyback converter are summarized in Table I.

The control waveform in DCM is shown in Fig. 3(c). Since i_L starts from zero in each switching cycle, it can be observed that d is independent of i_L and governed only by v_c and slopes of i_L and v_{ramp}. The DCM current mode control models have been reported in [4] and [6]. When applied to a flyback converter, these two models yield an almost identical result [7]. However, for sake of unified treatment, the DCM current-mode control model by Ridley [4] is used here, which is given by:

$$\hat{d} = F_m(\hat{v}_c + k'_f \hat{v}_{on} + k'_r \hat{v}_{off}) \tag{2}$$

Unlike its CCM counterpart in (1), there is no inductor current feedback in (2) and hence $H_e(s)$ is eliminated from the equation. The values of F_m, K'_r, and K'_f for a DCM flyback converter are provided in Table I.

C. Optocoupler Feedback

The optocoupler feedback with the TL431 error amplifier is shown in Fig. 4. With the reference voltage of TL431 being constant (i.e. $\hat{v}_{ref,TL431} = 0$), the following expressions can be written from the circuit in Fig. 4:

$$\frac{\hat{v}_{KD}}{\hat{v}_o} = \frac{R_{D2}}{R_{D1}+R_{D2}} \tag{3}$$

$$\frac{\hat{v}_K}{\hat{v}_{KD}} = -\frac{Z_2}{Z_1} \tag{4}$$

$$\hat{i}_{oc1} = \frac{\hat{v}_o - \hat{v}_K}{R_1} \tag{5}$$

$$\frac{\hat{i}_{oc2}}{\hat{i}_{oc1}} = CTR \tag{6}$$

$$\frac{\hat{v}_c}{\hat{i}_{oc2}} = -R_{C3} // \frac{1}{sC_{C3}} = Z_3 \tag{7}$$

From (3) to (7), the optocoupler feedback's transfer function is found to be

$$G_C(s) = \frac{\hat{v}_c}{\hat{v}_o} = -CTR(1+K_D\frac{Z_2}{Z_1})\frac{Z_3}{R_1} \tag{8}$$

where CTR is a current transfer ratio of the optocoupler,

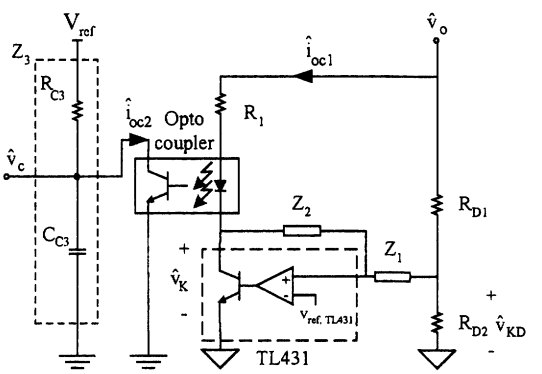

Figure 4. Optocoupler feedback circuit.

TABLE I. PARAMETERS IN CURRENT-MODE CONTROL MODELS

Mode	F_m	k'_f	k'_r	$H_e(s)$
CCM	$\frac{1}{(S_n+S_e)T_s}$	$-\frac{n^2DT_SR_S}{L}\left(1-\frac{D}{2}\right)$	$\frac{n^2D'^2T_SR_S}{2L}$	$1-\frac{T_s}{2}s+\frac{T_s^2}{\pi^2}s^2$
DCM	$\frac{1}{(S_n+S_e)T_s}$	$-\frac{n^2DT_SR_S}{L}$	0	0

$K_D = \frac{R_{D2}}{R_{D1}+R_{D2}}$ is the voltage divider gain, and Z_1, Z_2 and Z_3 (which is equal to R_{C3} parallel with $1/sC_{C3}$) are the controller impedance.

Usually, $K_D \frac{Z_2}{Z_1} >> 1$ in the range of frequencies of interest, thus (8) can be simplified into

$$G_c(s) = -CTR \cdot K_D \frac{Z_2}{Z_1}\frac{Z_3}{R_1} \qquad (9)$$

IV. Model Integration and Verification

Putting together the equivalent circuit in Fig. 2(a), (1), and (8), the block diagram of the flyback converter in CCM can be drawn as shown in Fig. 5(a). Similarly, combining the equivalent circuit in Fig. 2(b), (2) and (8), the block diagram of the converter in DCM is given in Fig. 5(b). In the case of DCM, the blocks associated with $\hat{i}_L$ disappears because $\hat{d}$ is independent of $\hat{i}_L$. The control-to-output transfer function ($G_{vc}(s) = \frac{\hat{v}_o}{\hat{v}_c}$) used in controller design can be derived from Fig. 5(a) and 5(b) by setting the input $\frac{\hat{v}_{in}}{n}$ in to zero.

The derivation of $G_{vc}(s)$ is illustrated with the prototype CCM and DCM flyback converters shown in Fig. 6, with the following specifications: V_{in} = 310V±10% (obtained from rectifying the AC mains of 220V±10%), V_o = 5V, I_o = 1-3A.

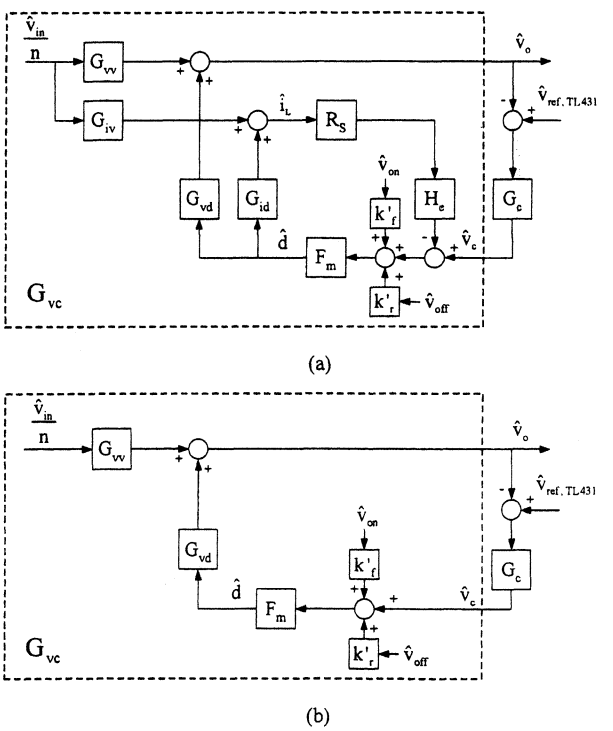

Figure 5. Block diagrams of a current-mode controller flyback converter with optocoupler feedback (a) CCM (b) DCM.

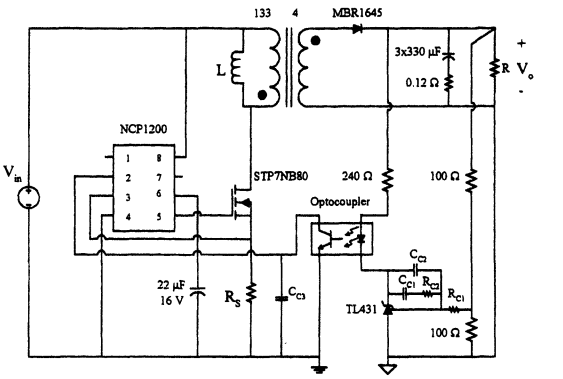

Figure 6. Prototype current-mode controlled flyback converter.

In the CCM circuit, L = 15mH and R_s = 2Ω, while in the DCM circuit, L = 3.7mH and R_s = 1Ω. Moreover, in the DCM circuit the component C_{C2} is excluded. A primary-to-secondary turn ratio is chosen at n = 33.25 in both prototype circuits. Current-mode control is implemented with the IC NCP1200 [8], which has a switching frequency f_s = 60kHz. Because the converters operate with d < 0.5, the compensation ramp therefore is not used (i.e. S_e = 0). With the given circuit parameters, inspection of the expressions for K'_f and K'_r in Table I found that their values are negligibly small and thus can be assumed to be zero in both CCM and DCM cases. Furthermore, the effect of $H_e(s)$ in the CCM current-mode control model can be omitted in practical controller design, i.e. $H_e(s)$ = 1, as the converter's crossover frequency is usually chosen to be well below $f_s/2$. Following these simplifications, $G_{vc}(s)$ can be derived from the models in Fig. 5. For CCM, it is given by

$$G_{vc}(s) = \frac{\hat{v}_o}{\hat{v}_c} = \frac{F_m G_{vd}(s)}{1 + F_m R_S G_{id}(s)} \qquad (10)$$

where $G_{vd}(s) = K_{vd}\frac{(1-\frac{s}{\omega_{zRHP}})(1+\frac{s}{\omega_{zc}})}{1+\frac{1}{Q}\frac{s}{\omega_o}+\frac{s^2}{\omega_o^2}}$, $K_{vd} = \frac{V_{in}}{nD'^2}$,

$Q = \frac{1}{\omega_o(\frac{L}{n^2D'^2R}+r_cR)}$, $\omega_{zRHP} = \frac{n^2D'^2R}{DL}$, $\omega_{zc} = \frac{1}{r_cC}$,

$\omega_o = \frac{n}{\sqrt{LC}}\sqrt{\frac{D'^2R}{R+r_c}}$, $G_{id}(s) = K_{id}\frac{1+\frac{s}{\omega_{z3}}}{1+\frac{1}{Q}\frac{s}{\omega_o}+\frac{s^2}{\omega_o^2}}$, $\omega_{z3} = \frac{1}{RC}$,

and $K_{id} = (1+\frac{2D}{D'})\frac{V_{in}}{nD'^2R}$. For DCM, it is given by

$$G_{vc}(s) = \frac{\hat{v}_o(s)}{\hat{v}_c(s)} = F_m G_{vd}(s) \qquad (11)$$

where $G_{vd}(s) = K_{vd}\frac{(1-\frac{s}{\omega_{zRHP}})(1+\frac{s}{\omega_{zc}})}{(1+\frac{s}{\omega_{p1}})(1+\frac{s}{\omega_{p2}})}$, $\omega_{zRHP} = \frac{n^2R}{LM(M+1)}$,

$K_{vd} = \frac{V_{in}}{n\sqrt{K}}$, $\omega_{zc} = \frac{1}{r_c C}$, $\omega_{p1} = \frac{2}{RC}$, $\omega_{p2} = \frac{n^2 R}{L(M+1)^2}$, and $M = \frac{V_o}{V_{in}}$.

Bode plots of (10) and (11) under the minimum input voltage (V_{in} = 280V) and maximum load current (I_o = 3A) are shown by the solid lines in Fig 7. $G_{vc}(s)$ in CCM has a zero due to the capacitor's ESR at f_{zc} =1.34kHz, a Right-Half-Plane (RHP) zero at f_{zRHP} = 21kHz, a low frequency pole at f_{pL} = 130Hz, a high frequency pole at f_{pH} = 19.90kHz, and a DC gain of –11.08dB. $G_{vc}(s)$ in DCM has a zero due to the capacitor's ESR at f_{zc} =1.34kHz, a Right-Half-Plane (RHP) zero at f_{zRHP} = 88.7kHz, a low frequency pole at f_{pL} = 192.57Hz, a high frequency pole at f_{pH} = 33.06kHz, and a DC gain of –7.99dB. To confirm the validity of these results, they are compared with the similar results obtained from SPICE simulation. In the SPICE simulation, the averaged models of the current-mode controlled flyback converters in CCM and DCM [6] were simulated (using .AC command); the corresponding results of $\frac{\hat{v}_o}{\hat{v}_c}$ are shown by the dashed lines in Fig. 7. It can be seen that the two results are closely agreed in both CCM and DCM cases, confirming the accuracy of the derived $G_{vc}(s)$ in (10) and (11).

V. Control Design

The control design principally involves determination of component values of the controller to give the converter satisfactory steady state and transient performances. Referring to the optocoupler feedback circuit in Fig. 4 and the prototype converter in Fig. 6, the controller in CCM consists of $Z_1 = R_{C1}$, $Z_2 = (1/sC_{C2})//(R_{C2}+1/sC_{C1})$, and $Z_3 = R_{C3}//(1/sC_{C3})$, and in DCM $Z_1 = R_{C1}$, $Z_2 = R_{C2}+1/sC_{C1}$, and $Z_3 = R_{C3}//(1/sC_{C3})$. Substituting the values of Z_1, Z_2, and Z_3 into (9), $G_c(s)$ for CCM is obtained as

$$G_c(s) = K_C \frac{(1+\frac{s}{\omega_Z})}{(\frac{s}{\omega_{P0}})(1+\frac{s}{\omega_{P1}})(1+\frac{s}{\omega_{P2}})} \quad (12)$$

where $K_C = \frac{CTR \cdot K_D R_{C3}}{R_1}$, $\omega_Z = \frac{1}{C_{C1}R_{C2}}$, $\omega_{P1} = \frac{1}{C_{C3}R_{C3}}$, $\omega_{P0} = \frac{1}{(C_{C1}+C_{C2})R_{C1}}$, $\omega_{P2} = \frac{C_{C1}+C_{C2}}{C_{C1}C_{C2}R_{C2}}$. And, $G_c(s)$ for DCM is obtained as

$$G_c(s) = K_C \frac{(1+\frac{s}{\omega_Z})}{(\frac{s}{\omega_{P0}})(1+\frac{s}{\omega_{P1}})} \quad (13)$$

where $\omega_{P0} = \frac{1}{C_{C1}R_{C1}}$ and K_C, ω_Z, and ω_{P1} are the same as those of CCM. It should be noted that R_{C3} = 8kΩ is located inside the NCP1200 and pulled up to the internal reference voltage V_{ref} = 5.2V (Fig. 4). The gain K_D is equal to 0.5 and the optocoupler is biased to operate with the current transfer ratio close to 100% (i.e. CTR ≈ 1). $G_c(s)$ of the CCM prototype circuit has one pole more than its DCM counterpart; this extra pole is used to suppress gain peaking at $f_s/2$ caused by sampling action in the current loop ($H_e(s)$). In both cases, $G_c(s)$ contains an integrator, which will help boost DC gain of the converters, thus enhancing output voltage regulation.

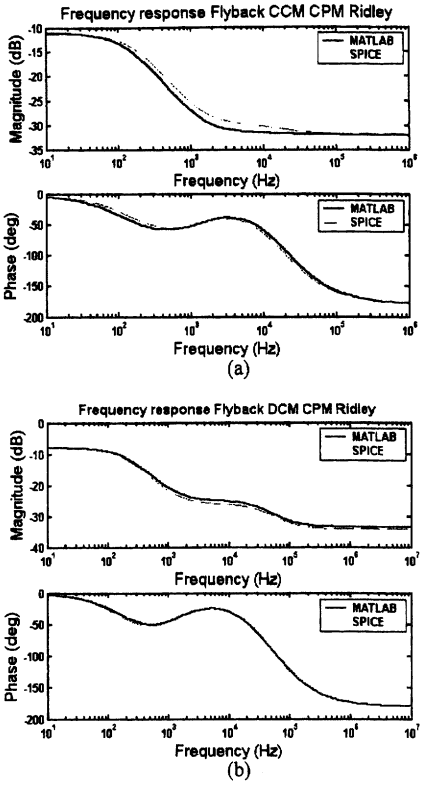

Figure 7. Bode plots of $G_{vc}(s)$ (a) CCM (b) DCM.

In control design, the crossover frequency, f_c, is chosen at 1kHz. In the CCM prototype, the $G_c(s)$'s zero is placed at f_z = 130Hz (coincide with the f_{pL} of $G_{vc}(s)$ in (10)), the first pole at the origin, and other two poles at $f_{p1} = f_{p2}$ = 1.30kHz (near f_{zc}). Consequently, the compensation circuit component values are calculated and rounded off to the nearest standard values, obtaining R_{C1} = 6.8kΩ, R_{C2} = 15kΩ, R_{C3} = 8kΩ, C_{C1} = 82nF, C_{C2} = 10nF, and C_{C3} = 15nF. In the DCM prototype, the $G_c(s)$'s zero is placed at f_z = 200Hz (near the f_{pL} of $G_{vc}(s)$ in (11)), the first pole at the origin, and another pole at f_{p1} = 1.30kHz (near f_{zc}). As a result the following component values are obtained: R_{C1} = 5kΩ, R_{C2} = 3.9kΩ, R_{C3} = 8kΩ, C_{C1} = 220nF, and C_{C3} = 15nF. Fig. 8 shows Bode plots of the open loop transfer function, $G_{vc}(s)G_c(s)$. The solid lines represent the plot under minimum input voltage and maximum load current condition, while the dashed line under maximum input voltage and minimum load current condition. It can be seen that the designed controllers yield the stable systems, with phase margin of about 45° in the CCM converter and about 90° in the DCM converter. In Fig 8(a), the attenuation of $G_{vc}(s)G_c(s)$ at

$f_s/2$ (30kHz) is over –50dB. This substantial attenuation, achieved due to the placement of the controller's poles at f_{p1} and f_{p2}, will ensure the effective gain damping in CCM at $f_s/2$.

To verify the performance of the designed controllers, the prototype flyback converters were subjected to a step-load, with the results shown in Fig. 9. The output voltage's recovering time of the CCM and DCM converters is measured to be 400μs and 300μs respectively. Despite an integral action of the controllers, the steady state error nevertheless is noticeable when the load current is 3A. This error may be due to the limited performance of the TL431 error amplifier.

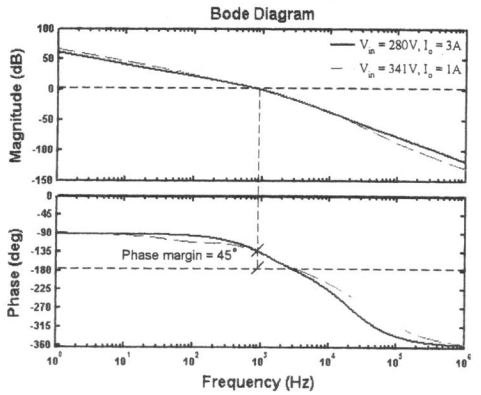

(a)

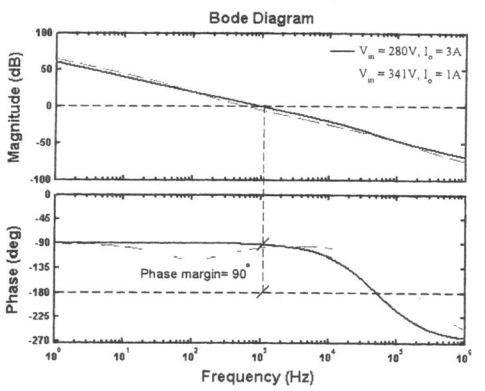

(b)

Figure 8. Bode plots of the open loop transfer function, $G_{vc}(s)G_c(s)$, (a) CCM (b) DCM.

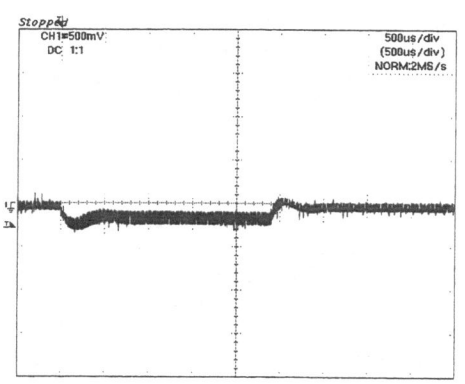

(a)

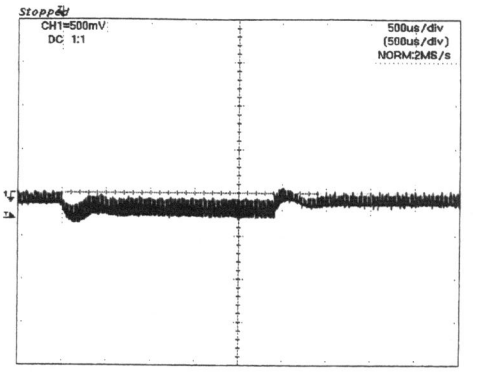

(b)

Figure 9. Measured output voltage response when the load current is stepped back and forth between 1A and 3A (a) CCM (b) DCM.

VI. CONCLUSION

Modeling and control design of a current-mode controlled flyback converter with optocoupler feedback have been presented in this paper. The modeling procedure is the same in both CCM and DCM and essentially involves substitution of flyback power stage, current-mode control stage, and optocoupler feedback stage by their respective small-signal models. The control-to-output transfer function, $G_{vc}(s)$, was derived from the combined power circuit and current-mode control models. The derived $G_{vc}(s)$ was found to be consistent with the result from SPICE simulation, confirming its validity to be used in control design. Based on the derived $G_{vc}(s)$, the controller design was carried out for the CCM and DCM prototype converters. The experimental results show that the designed controllers provide the converters with satisfactory performance.

REFERENCES

[1] T.H. Chen, W.L. Lin, and C.M Liaw, "Dynamic modeling and controller design of flyback converter ", IEEE Trans. Aerospace and Electronic Systems, vol. 35, no. 4, pp. 1230-1238, 1999.

[2] V. Vorperian, "Simplified analysis of pwm converter using model of pwm switch: part I and II", IEEE Trans. on Aerospace and Electronic Systems, vol. 26, no. 3, pp. 490-505, 1990.

[3] R. B. Ridley, "A new continuous-time model for current-mode control", IEEE Trans. on Power Electronics, vol. 6, no. 2, pp. 271-280, 1991.

[4] R. B. Ridley, "A new continuous-time model for current-mode control with constant frequency, constant on-time, and constant off-time, in CCM and DCM", Proceedings Power Electronics Specialists Conference, pp. 382-389, 1990.

[5] Y. Panov and M. Jovanovic, "Small-Signal analysis and control design of isolated power supplies with optocoupler feedback", Proceedings Applied Power Electronics Conference and Exposition, pp. 22-26, 2004.

[6] R. W. Erickson and D. Maksimovic, Fundamentals of Power Electronics", 2nd ed., Kluwer Academic Publishers, 2001.

[7] W. Kleepchampee, "Modeling and controller design of a current-mode controlled flyback converter with optocoupler feedback", Master Thesis, King Mongkut's Institute of Technology Ladkrabang, 2005.

[8] NCP1200 Literature Pack, ON Semiconductor, 2001.